Ag/SeO₂/C Avalanche Type Resonant Tunneling Schottky Barriers

Sabah E. Al Garni[a], A.F. Qasrawi[b,c,*] ⓘ***, Najla M. Khusayfan[a]***

[a]*University of Jeddah, Faculty of Science, Department of Physics, Jeddah, Saudi Arabia.*
[b]*Arab American University, Department of physics, Jenin 240, Palestine.*
[c]*Istinye University, Department of Electrical and Electronics Engineering, 34010, Istanbul, Turkey.*

Herein, the design and characterization of Ag/SeO₂/C avalanche type resonant tunneling devices are reported. Thin pellets of SeO₂ nano-powders pressed under hydraulic pressure of 1.0 MPa which is used as the active material are characterized. They showed tetragonal structure refereeing to space group of $P_{4_2 mbc}$ and lattice parameters of $a = b = 7.866$ Å and $c = 5.336$ Å. The current-voltage characteristic curves have shown that SeO₂ can perform as active media to produce resonant tunneling diodes when forward biased and as avalanche type diode when reverse biased. The peak to valley current ratios of these diodes reached 18.3. In addition, the impedance spectroscopy measurements have shown that the device works in the low impedance mode when operated in the microwave range of frequency near 1.50 GHz. Negative conductance effect is observed in that frequency domain. The features of the Ag/SeO₂/C nominate them for use as signal amplifiers and microwave oscillators.

Keywords: *Ag/SeO₂/C; tetragonal; microwave cavity; Esaki diodes; negative conductance.*

1. Introduction

Selenium dioxide based ceramics has attracted the attention of many researchers due to their wide range of applications in various technology sectors. As for examples, they are used for advanced shielding applications[1]. They also find applications as electrocatalysts[2]. Literature data reported thousands of articles about many technological applications that benefits from selenium dioxide as selenating agent under simple reacting conditions[3]. However, articles which consider SeO₂ as a solid compound suitable for electronic applications are almost absent. For this reason, we are motivated to find new class of applications for this compound. Particularly, here in this work, we are going to produce thin pellets of SeO₂ powders and study their structural, morphological, compositional and electrical properties. The study will allow suggesting practical electronic applications for SeO₂. We are reporting results that show the selenium dioxide as active material similar to SiO₂ and MoO₃[4,5]. The latter materials capture the focus of thin film transistor technology designers. As for examples, carbon nanotubes (CNT)/SiO₂/MoO₃ is found ideal composite for charge storage. When used as electrodes in Li batteries it showed high specific capacity up to 0.7 Ah/g over 500 cycles[4]. In addition, stacked layers of Yb/MoO₃/In₂Se₃/Ag thin film transistors are mentioned capable of handling more than one duty at a time. These duties include bandpass/reject filter characteristics in the microwave range of frequency domain and visible light communication signal receivers[5].

2. Experimental Details

Powders of high purity of SeO₂ (99.99%, Alpha Aeser) were hydraulically pressed at 1.0 MPa in the shape of pellets of diameter of 1.2 cm and thickness of 0.12 cm. Electrical contacts to the SeO₂ pellets were actualized by using silver at the bottom and carbon point contact on top surface. The top diode area was 3.14×10^{-2} cm². The crystalline nature and morphology of the SeO₂ pellets was tested with Miniflex 600 X-ray diffraction unit and with Coxem 200 scanning electron microscope equipped with EDAX energy dispersive X-ray spectrometer. Electrical measurements were handled with automated Keithley Current-voltage characteristic system and Agilent 4291B 0.01-1.80 GHz impedance analyzer.

3. Results and Discussion

The results of the X-ray diffraction measurements on SeO₂ samples are shown in Figure 1a. It is clear from the figure that the samples exhibit polycrystalline nature. An analysis of the XRD patterns which were carried out with "Crystdiff" software packages have shown that the powder based samples prefers crystallization in tetragonal phase corresponding to the space group $P_{4_2 mbc}$ with lattice parameters of $a = b = 7.866$ Å and $c = 5.336$ Å. The lattice parameters are consistent with literature data in which values of $a = b = 8.263$ Å and $c = 5.033$ Å are obtained at pressure of 0.9 GPa[6,7]. The structural parameters presented by the crystallite size ($D = \frac{0.94\,\lambda}{\beta\,cos\theta}$; β: maximum peak broadening[8]), strain ($\varepsilon = \frac{\beta}{4 tan\theta}$, staking faults ($SF\% = \frac{2\pi^2 \beta}{45\sqrt{3 \tan(\theta)}}$[8]), dislocation density ($\delta = \frac{15\,\varepsilon}{a\,D}$[8]) which are calculated from the maximum peak provide evidences
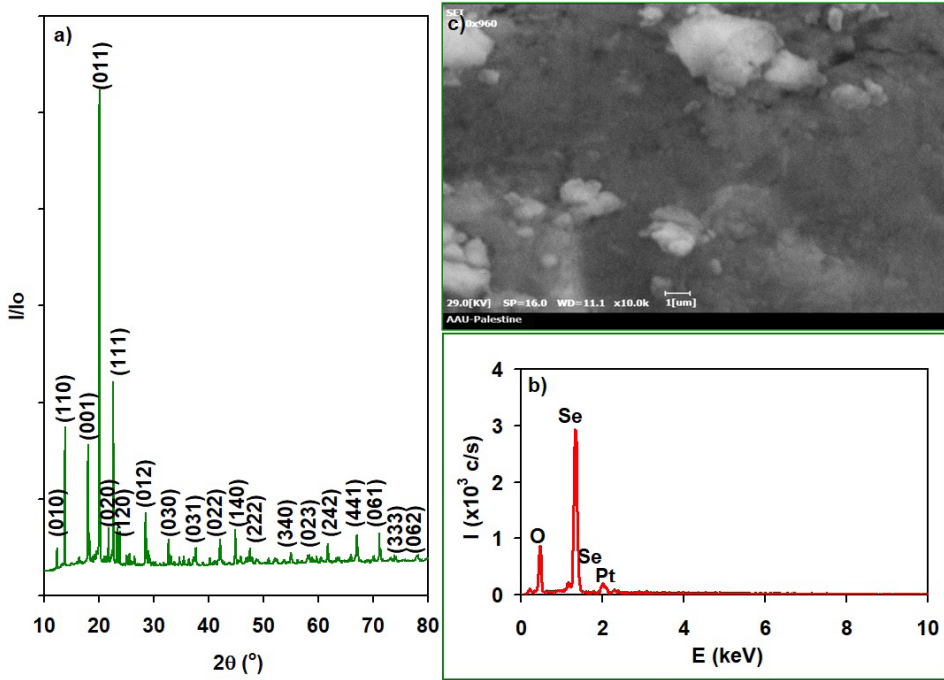
Figure 1. (a) the X-ray diffraction and (b) the dispersive X-ray spectra and (c) the scanning electron microscopy images for the SeO_2 pellets.

about the structural properties. Namely, the samples under study displayed $D = 67$nm, $\varepsilon = 3.08 \times 10^{-3}$, $SF\% = 0.131\%$ and $\delta_a = 8.69 \times 10^{10}$ lines/cm². Compared to literature data, the crystallite sizes and dislocation density values of the SeO_2 pellets are sufficient to explain their physical properties using band theory of solids. These two structural parameters also allow application of these pellets in optoelectronic technology[9,10].

Figure 2b show the results of the energy dispersive X-ray spectroscopy for the SeO_2 pellets. It is clear from the spectra that the material is composed of Se, O and Pt only. Platinum appears because it was coated onto the pellets to prevent electron contaminations. In general, SeO_2 samples are pure and exhibit homogeneous stoichiometry in all parts of the sample. Energy dispersive X-ray spectroscopy (EDS) revealed compositional ratios of 62.2 at% Se and 37.8 at. % O. The data suggested some oxygen deficiency in the samples. On the other hand, the scanning electron microscopy images (SEM) for the studied samples are illustrated in Figure 1c. In accordance with SEM images which represent an enlargement by 10000 times, the surface is continuous and almost no cracks existed in the samples.

The hot probe technique has the *p*-type conductivity of SeO_2. As shown in the energy band diagram presented in Figure 2a, from electronic point of view, as the electron affinity and energy band gap of SeO_2 are 1.89 eV[11] and 3.70 eV[12,13], respectively, the work function $(q\phi_s = q\chi + E_g - (E_{FP}))$[14] of SeO_2 is located below the middle of the energy band gap $(E_i = E_g/2)$. Since the work function is larger than $(q\phi_s > (q\chi + E_i))$ 3.75 eV and less than $(q\phi_s < (q\chi + E_g))$ 5.60 eV, any metal of $3.75 < q\phi_m < 5.60$ eV could possibly perform as Schottky contact with SeO_2[14]. However, the energy band gap of SeO_2 is mentioned containing energy band
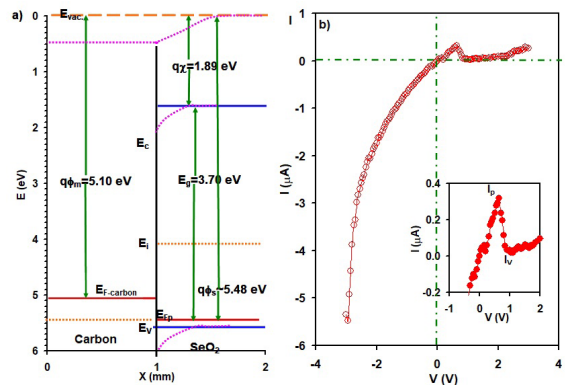
Figure 2. (a) the energy band diagram and (b) the current-voltage characteristics for $Ag/SeO_2/C$ diodes. The inset of (b) shows an enlargement of the forward current.

tails of width of 0.12 eV[13]. These band tails could behave as electron/hole centers forcing the Fermi level to be located near these localized states (very close to the valence band). Thus, it is reasonable to assume work functions of values of ~5.48 eV. While coating SeO_2 pellets with Ag resulted in an ohmic nature of contact, carbon $(q\phi_C = 5.10$ eV[15]) results in Schottky type metal-semiconductor interfaces[14]. As can be seen from the band diagram shown in Figure 2a, the built in potential of the device $(qV_{bi} = q\phi_s - q\phi_m)$ is ~0.38 eV. Demonstration of the possible formation of the Schottky diodes is verified via the current-voltage characteristic curves which are shown in Figure 2b. The figure indicates avalanche type diodes in which large leakage current prevails[14]. Avalanche multiplication of the holes and electrons

is created by ionization process under the influence of high electric fields. They are important devices for microwave oscillation. In these diodes applying large reverse voltage across the diode terminals widens the space charge region from the p^+ side (majority carriers in SeO$_2$) to the minority carriers (n) region. This is called reach through condition. It states that as the reverse voltage increases, the reverse-biased depletions region will eventually reach through to the forward-biased depletion region. As also illustrated in the inset of Figure 2b, when the C/SeO$_2$ avalanche diodes are forward biased, the current show peaky behavior in which it initially rises reaching a maxima of ($I_p = 0.32 \ \mu A$) at $V_p = 0.65$V. Applying larger forward voltages resulted in decrease in the current values until the valley point ($I_v = 17$nA) is reached at $V_v = 1.10 \ V$. The peak to valley current ratios ($PVCR = \frac{I_p}{I_v}$) is 18.3. This ratio is high enough to nominate the C/SeO$_2$ avalanche diodes for use as resonant tunneling diodes (RTD)[14]. $PVCR$ of 6.2 is reported for AlSb/GaInAsSb quantum well RTD's[16]. $PVCR$ of 62 was also observed for Ge/BN interfaces[17]. These types of devices occupy large space in communication technology as they are sources of negative conductance which is a main factor in Gigahertz/terahertz communication technology[14,18,19]. Particularly, when a system operates in the region of negative differential conductivity (NDC), where current falls rather than rises with increasing electric field, the density of carriers and their drift mobility strongly affects the NDC effect. Under conditions of NDC there is a tendency to enhance nonuniformities

that would otherwise be damped. As for examples, in the Gunn effect charge carriers exists in high and low states of mobility. Charge carriers in the high state of mobility move easier through the pellets than charge carriers of low mobility. When the pellets are unbiased most of the charge carriers exist in high mobility state. Applying a voltage to the samples, forces current flows from high mobility states. Gunn effect dominates when a sufficiently large voltage is applied forcing motion of charge carriers into the state of lower mobility. This leads them moving more slowly and decreasing the electrical conductivity of the material is observed[20]. As an avalanche effect, large voltage biasing is expected to be associated with large electrical current values. However, the ability of the nonmetallic solids to carry this huge current is limited by the scarcity of mobile charge carriers (hence current decreases with increasing applied voltage leading to negative differential conductance). Strong applied electric fields frees large number of charge carriers from the structure of the solid (impact ionization) and large current dominates again[14].

On the other hand fitting the reverse current as function of applied reverse voltage (inset of Figure 3a) showed a nonlinear quadratic relation. Namely, the reverse current is given by $I(V) = 0.27V^2 + 0.31V + 0.06$ in μA. This relation assures the valance multiplication effect in the diodes under study.

It is well known that the avalanche breakdown happens when a high reverse voltage is applied across the terminal of (Ag/SeO$_2$/C) diodes. As the reverse applied voltage is increased, the electric field across the junction increases.
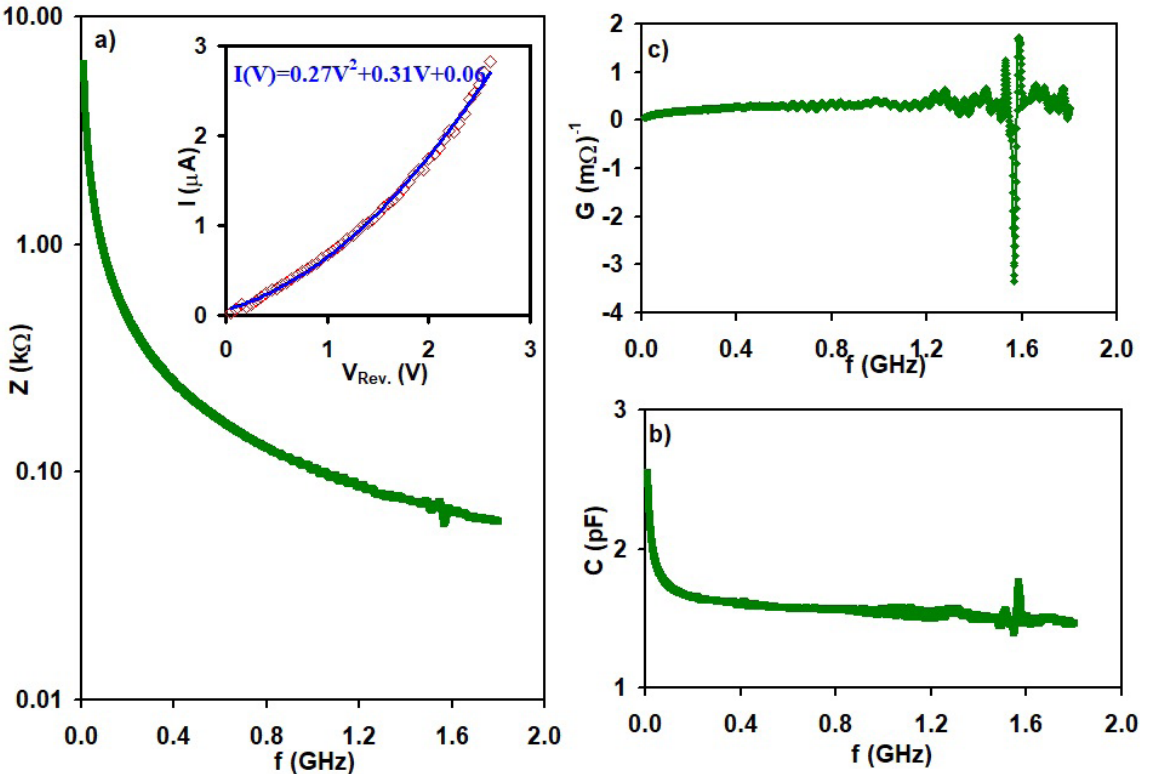
Figure 3. (a) the impedance, (b) the capacitance and (c) the conductance spectra for the Ag/SeO$_2$/C diodes. Inset of (a) showing the quadratic fitting of the reverse current as function of reverse voltage (V$_{Rev.}$).

This electric field exerts a force on the charge carriers at the junction and frees them from covalent bonds. These freed charge carriers start moving with high velocity across the junction and collide with the other atoms, thus creating freer carriers resulting in a rapid increase in net current. The other possible mechanism for the large reverse current is the Zener breakdown. Namely, when the device is reverse biased, the kinetic energy of the carriers increases. The high-velocity carriers collide with other atoms and give rise to other free carriers. These free carriers, in turn, give rise to a high value of reverse saturation current. The main difference between Zener breakdown and avalanche breakdown is their mechanism of occurrence. Zener breakdown occurs because of the high electric field. The avalanche breakdown occurs because of the collision of free electrons with atoms. Both these breakdowns can occur simultaneously[14].

As practical application of the C/SeO_2 avalanche/RTDs we have recorded the impedance spectra. The measured impedance (Z) capacitance (C) and conductance (G) spectra are shown in Figure 3a, b and c, respectively. It is clear from Figure 3a that the higher the signal frequency is, the lower the impedance value. Z decreases by two orders of magnitude as the frequency is increased from the radiowave (0.01 GHz) to the microwave frequency domain (~1.80 GHz). Low impedance in the microwave frequency domain is necessary for signal amplification especially in 5G mobile technologies[21]. They are employed to realize shunt capacitance in circuits[22]. As it is also readable from Figure 3b, the capacitance spectra follow the same trend of variation like that of impedance spectra. Namely, in the radiowave frequency domain, C sharply falls with increasing f. When the microwave frequency domain is reached, C slowly vary tending to remain constant. As the increasing f reaches 1.50 GHz, resonance-antiresonance peaks are observed. On the other hand, the conductance spectra which is the harvest of RTD, tends to remain positive and constant in the frequency domain of 0.01-1.50 GHz. When f >1.56 GHz, the conductance show negative values. As seen from Figure 3c, the narrow peak exhibit minimum at 1.56 GHz. Negative conductance (NG) effects is observed. NG effects and resonance-antiresonance in the capacitance was previously observed in Se/Se stacked layers comprising Ag nanosheets in is structure[23]. It is a sign of resonant tunneling diodes and beneficial for supplying the electronic circuits with energy for maintaining microwave oscillations[24]. It can also be employed for compensating the loss from the inductor-capacitor tank during resonance[25]. NG effect is believed to originate from the existence of large density of deep states within a narrow energy range above the valence band[26]. It could also originate from the avalanche effect which we observed in this work.

4. Conclusions

In the current work, we have shown that thin SeO_2 pellets which exhibit tetragonal structure can be employed as an electronic device. The electrical characterizations have shown that $Ag/SeO_2/C$ structure exhibit resonant tunneling diode characteristics with peak to value current ratios of 18.3. The devices also behaved as sources of negative conductance which can be used to compensate losses in microwave resonators (inductor-capacitor tanks). The devices showed wide transient impedance tunability making it suitable for microwave oscillations.

5. Acknowledgements

6. References

1. Elshami W, Tekin HO, Al-Buriahi MS, Hegazy HH, Abuzaid MM, Issa SA, et al. Developed selenium dioxide-based ceramics for advanced shielding applications: Au2O3 impact on nuclear radiation attenuation. Results in Physics. 2021;24:104099.

2. Swathi S, Rani BJ, Ravi G, Yuvakkumar R, Hong SI, Velauthapillai D, et al. Designing rational and cheapest SeO2 electrocatalyst for long stable water splitting process. J Phys Chem Solids. 2020;145:109544.

3. Marpna ID, Wanniang K, Lipon TM, Shangpliang OR, Myrboh B. Selenocyanation of aryl and styryl methyl ketones in the presence of selenium dioxide and malononitrile: an approach for the synthesis of α-carbonyl selenocyanates. J Org Chem. 2020;86(2):1980-6.

4. Zheng Y, Liu Z, Liu B, Wang S, Xiong C. Fabrication of cactus-like CNT/SiO2/MoO3 ternary composites for superior lithium storage. Energy. 2021;217:119386.

5. Qasrawi AF, Yaseen NM. Yb/MoO 3/In 2 Se 3/Ag sensors designed as tunneling diodes, MOSFETs, microwave resonators, laser sensors, and VLC receivers suitable for 4G/5G and VLC technologies. IEEE Trans Electron Dev. 2021;68(12):6444-50.

6. Grzechnik A, Farina L, Lauck R, Syassen K, Loa I, Bouvier P. Pressure-induced structural deformations in SeO2. J Solid State Chem. 2002;168(1):184-91.

7. Zak Z. Crystal structure of diselenium pentoxide Se2O5. Z Anorg Allg Chem. 1980;460(1):81-85.

8. AlGarni SE, Qasrawi AF. Indium slabs induced structural phase transitions and their effects on the electrical and optical properties of stacked layers of the thermally annealed Cu2O thin films. Results Phys. 2020;16:102901.

9. Yewale MA, Sharma AK, Kamble DB, Pawar CA, Potdar SS, Karle SC. Electrochemical synthesis of CuSxSe1-x thin film for supercapacitor application. J Alloys Compd. 2018;754:56-63.

10. Jung D, Herrick R, Norman J, Turnlund K, Jan C, Feng K, et al. Impact of threading dislocation density on the lifetime of InAs quantum dot lasers on Si. Appl Phys Lett. 2018;112(15):153507.

11. Behrens RG, Lemons RS, Rosenblatt GM. Vapor pressure and thermodynamics of selenium dioxide. The enthalpy of atomization of SeO2 (g). J Chem Thermodyn. 1974;6(5):457-66.

12. Thakur S, Kaur A, Singh L. Mixed valence effect of Se6+ and Zr4+ on structural, thermal, physical, and optical properties of B2O3–Bi2O3–SeO2–ZrO2 glasses. Opt Mater. 2019;96:109338.

13. Alharbi SR, Qasrawi AF, Algarni SE. Growth and characterization of (glass, Ag)/SeO2 thin films. Physica B. 2022;633:413790.

14. Sze SM, Li Y, Ng KK. Physics of semiconductor devices. Hoboken: John Wiley & Sons; 2021.

15. Khanfar HK, Qasrawi A, Daraghmeh M, Abusaa M. Structural and electrical characterizations of the as grown and annealed Au/MoO3/In/MoO3/C bandpass filters. Microw Opt Technol Lett. 2019;61(12):2866-72.

16. Guarin Castro ED, Rothmayr F, Krüger S, Knebl G, Schade A, Koeth J, et al. Resonant tunneling of electrons in AlSb/GaInAsSb double barrier quantum wells. AIP Adv. 2020;10(5):055024.

17. Al Garni SE, Qasrawi AF. Design and characterization of (Al, C)/p-Ge/p-BN/C isotype resonant electronic devices. Phys Status Solidi. 2015 Aug;212(8):1845-50.

18. Wang D, Chen Z, Su J, Wang T, Zhang B, Rong X, et al. Controlling phase-coherent electron transport in III-nitrides: toward room temperature negative differential resistance in AlGaN/GaN double barrier structures. Adv Funct Mater. 2021;31(8):2007216.

19. Lee J, Kim M, Yang KA. 1.52 THz RTD Triple-Push Oscillator With a $\mu {\hbox {W}} $-Level Output Power. IEEE Trans Terahertz Sci Technol. 2015;6(2):336-40.

20. Conwell EM. Negative differential conductivity. Phys Today. 1970;23(6):35.

21. Zhou J, Chen W, Chen L, Feng Z. 3.5-0Hz high-efficiency broadband asymmetric doherty power amplifier for 5G applications. In 2018 International Conference on Microwave and Millimeter Wave Technology (ICMMT); 2018 May 7; USA. Proceedings. USA: IEEE. p. 1-3.

22. Vaezi A, Gharaklili FG. Synthesis and design of an LPF with wide-stop band and high rejection level. AEU Int J Electron Commun. 2018;95:139-45.

23. Qasrawi AF, Aloushi HD. Formation, negative capacitance and negative conductance effects in Selenium stacked layers sandwiched with Ag nanosheets. Mater Res Express. 2019;6(8):086435.

24. Guo M, Xue Y, Gao Z, Zhang Y, Dou G, Li Y. Dynamic analysis of a physical SBT memristor-based chaotic circuit. Int J Bifurcat Chaos. 2017;27(13):1730047.

25. Jang SL, Liu CC, Huang JF. A wide locking range injection locked frequency divider with quadrature outputs. IEICE Trans Electron. 2008;91(3):373-7.

26. Pan JL, McManis JE, Grober L, Woodall JM. Gallium-arsenide deep-level tunnel diode with record negative conductance and record peak current density. Solid-State Electron. 2004;48(10-11):2067-70.